Research Square

Preprints are preliminary reports that have not undergone peer review.
They should not be considered conclusive, used to inform clinical practice,
or referenced by the media as validated information.

Multi-Objective Design of Combined Drainage Systems in Homogeneous Earth Dams Using Finite-Element, Pareto, and TOPSIS Methods

Ahmad Reza Mazaheri

a.mazaheri@abru.ac.ir

Ayatollah Borujerdi University

Behrang Beiranvand

Ayatollah Borujerdi University

Research Article

Keywords: Earth dam, Horizontal blanket drain, Toe drain, Pareto ranking, TOPSIS, Finite-element analysis

Posted Date: November 24th, 2026

DOI: https://doi.org/10.21203/rs.3.rs-11743863/v1

License: This work is licensed under a Creative Commons Attribution 4.0 International License.
Read Full License

Additional Declarations: No competing interests reported.

Multi-Objective Design of Combined Drainage Systems in Homogeneous Earth Dams Using Finite-Element, Pareto, and TOPSIS Methods

Ahmad Reza Mazaheri[1,*], **Behrang Beiranvand**[1]

[1] Department of Civil Engineering, Faculty of Engineering, Ayatollah Borujerdi University, Borujerd, Lorestan, Iran

*** Corresponding author: Ahmad Reza Mazaheri, a.mazaheri@abru.ac.ir**

Co-author e-mails: behrang220@gmail.com (B. Beiranvand)

Focus area: Surface and subsurface water resources engineering

Article type: Research article

Abstract

Internal drainage in earth dams must improve downstream stability without causing unnecessary seepage discharge. A coupled finite-element framework was developed for the design of a horizontal blanket connected to a downstream toe drain in homogeneous earth dams. Three embankment heights (15, 25, 35 m) and two downstream slopes (1V:1.5H, 1V:2H) were analysed in ABAQUS under steady-state seepage. Design variables were the normalized blanket length (d/N), toe-drain height ratio (h/H) and blanket thickness (b). The downstream factor of safety (FOS) was obtained by strength reduction, and Q is the steady-state seepage discharge per unit width. Simulated designs were ranked by fast non-dominated sorting and crowding distance (NSGA-II framework), and the Technique for Order of Preference by Similarity to Ideal Solution (TOPSIS) selected a compromise solution from the non-dominated set. Grey Wolf Optimizer-tuned Random Forest surrogates served only for a within-boundary consistency check. The ratio h/H was the strongest control on FOS: raising it from 0.10 to 0.30 increased FOS by up to about 24% for short blankets, whereas the response to blanket length diminished beyond d/N ≈ 0.4–0.5. A 2.5-fold increase in blanket thickness changed FOS by only about 2.1%. The Pareto sets concentrated near d/N = 0.50–0.60 and h/H = 0.25–0.30 for the 25 and 35 m dams, while the 15 m cases spanned h/H = 0.10–0.30. The surrogates reproduced FOS better than Q (weakest case: Q for 35 m, 1V:1.5H, testing $R^2 = 0.46$). The resulting ranges are preliminary, model-specific design bands rather than universal optima.

Keywords: Earth dam; Horizontal blanket drain; Toe drain; Pareto ranking; TOPSIS; Finite-element analysis

1. Introduction

Seepage control is a central component of earth-dam safety because elevated pore-water pressures can reduce the effective stress in the downstream shell and alter the conditions governing slope instability. Drainage systems are therefore designed to intercept seepage, lower the phreatic surface, and manage downstream pore-water pressures. Recent numerical and experimental studies confirm that drain geometry, hydraulic conductivity contrasts, and boundary conditions can substantially affect both seepage discharge and stability, while the performance of a drainage configuration remains strongly dependent on dam geometry and material conditions (Siacara et al. 2022; Soualhi and Benmebarek 2022; Mostafa and Zhenzhong 2023a; Amieur et al. 2023; Al-Janabi et al. 2025).

Earlier studies established the importance of horizontal-drain length and downstream drain geometry for seepage control in homogeneous and zoned earth dams (Chahar 2004; Calamak et al. 2018; Refaiy et al. 2021; Charrak et al. 2025). More recent investigations have compared alternative drainage arrangements and optimization strategies, including parallel drains, vertical drains, and drainage systems selected through numerical optimization (Soualhi and Benmebarek 2022; Zakaria and Mahmood 2023; Amieur et al. 2023; Parsaie et al. 2025). Finite-element stability formulations have also been extended to alternative failure criteria and coupled numerical settings (Mouyeaux et al. 2023), supporting the use of a consistent hydro-mechanical framework when drainage geometry is varied.

Recent work has moved beyond seepage-only assessment toward coupled or comparative analyses of seepage and stability. Finite-element and numerical studies have examined internal cutoff walls, drain location and diameter, diaphragm cracking, and transient or reliability-based seepage conditions (Haghdoost et al. 2023; Hassan et al. 2024; Fawzy et al. 2024; Pourbeirak et al. 2026). Field-oriented studies have likewise emphasized that seepage monitoring and internal instability are relevant to long-term dam safety, particularly where hydraulic gradients and drainage performance evolve with time (Lee et al. 2024; Radzicki and Stoliński 2024; Fontanella et al. 2025). These studies reinforce the need to distinguish the hydraulic benefit of a drain from its consequences for the stability response.

The optimization problem is inherently multi-objective. Increasing drainage dimensions can improve stability or reduce internal pore-water pressures, but it may also alter the collected discharge, the construction requirements, and the location of the seepage boundary. Simulation–optimization studies have demonstrated the value of combining finite-element seepage calculations with an explicit design-search layer, while recent reviews emphasize that the optimum drainage configuration is case dependent rather than universal (Hassan et al. 2022, 2023; EL-Molla and Kilit 2026; Al-Juboori and Datta 2019). In this context, Pareto ranking is useful for identifying non-dominated alternatives, whereas the Technique for Order of Preference by Similarity to Ideal Solution (TOPSIS) can provide a transparent decision layer when the designer must select one compromise from a non-dominated set.

Finite-element databases can also become computationally expensive when several geometric variables and dam configurations are explored. Machine-learning surrogates have consequently been applied to dam seepage, pore-pressure, and slope-stability problems, including Random Forest (RF), neural networks, and hybrid optimization frameworks (Breiman 2001; Huang et al. 2023; Wise et al. 2023; Chen et al. 2024; He and Wu 2023; Rehamnia and Mahdavi-Meymand 2025; Arabet et al. 2025). For geotechnical prediction, ensemble models and metaheuristic hyperparameter optimization have also been investigated, including RF combined with swarm-based optimizers (Bardhan et al. 2024; Wang et al. 2024; Kadkhodaei et al. 2025). These studies support the use of surrogate models as computational accelerators, but they also show why validation and an explicit separation between the numerical reference model and the surrogate are essential.
The methodological gap addressed here is narrower than a claim of universal optimization: the present study evaluates, within one consistent two-dimensional finite-element database, how toe-drain elevation, horizontal-blanket length, and blanket thickness jointly affect downstream factor of safety (FOS) and seepage discharge for homogeneous dams of different heights and downstream slopes. The design database is first ranked directly from the finite-element results; TOPSIS is then positioned as a decision layer rather than as a replacement for Pareto dominance. Finally, a Grey Wolf Optimizer (GWO)-RF model is used only to densify the sampled design space inside the original bounds and to test whether the qualitative Pareto pattern persists between sampled points. This separation is important because recent reliability and machine-learning studies show that uncertainty, sampling strategy, and validation can materially influence surrogate-based conclusions (Huang et al. 2025; Yu et al. 2025).

2. Materials and Methods

2.1. Geometrical configuration and design variables

Homogeneous embankments were adopted to isolate the influence of drainage geometry without introducing additional effects from core–shell interfaces. The drainage system consists of a horizontal blanket connected to a downstream toe drain (Fig. 1). Three embankment heights, $H = 15$, 25, and 35 m, were considered with downstream slopes of 1V: 1.5H and 1V: 2H. Crest widths were fixed at 5, 7.5, and 10 m, respectively. The principal design variables are the horizontal blanket length d, the blanket thickness b, and the toe-drain height h. The normalized variables are d/N and h/H, where N is the horizontal distance from the downstream crest edge to the downstream toe. For a downstream slope of 1V: mH, the horizontal projection is given by:

$$N = mH \qquad (1)$$

The design ranges were $d/N = 0.10$–0.60 (dimensionless), $b = 1.0$–5.0 m (with a baseline $B = 2$ m, so that $b/B = 0.5$–2.5), and $h/H = 0.10$–0.40 (dimensionless). Importantly, the $h/H = 0.10$–0.30 range is used in the main FOS sensitivity and Pareto analysis shown in Fig. 4 and Table 2, whereas Figs. 5 and 6 extend the hydraulic sensitivity analysis to $h/H = 0.40$. This distinction removes any ambiguity between the parametric and Pareto databases.

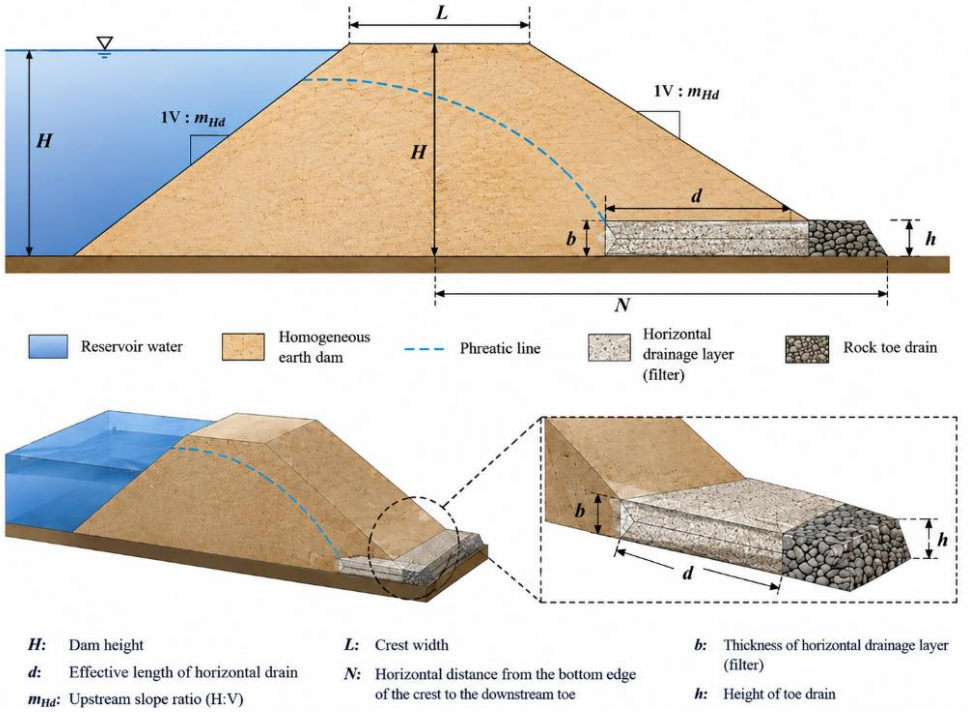


Fig. 1 Schematic cross-section of the homogeneous earth dam with a combined horizontal-toe drainage system and the principal design variables

2.2. Finite-element seepage and hydro-mechanical formulation

The numerical analyses were performed in ABAQUS using coupled pore-fluid-displacement elements. The hydraulic field was solved under steady-state conditions, while the coupled formulation accounts for the interaction between pore pressure and the deformable soil skeleton. Darcy flow was used for the porous medium, and the soil skeleton was represented by an elastoplastic Mohr–Coulomb model. The governing hydraulic relation is expressed as:

$$\mathbf{q} = -\mathbf{K}\nabla h \qquad (2)$$

where $\mathbf{q}$ is the Darcy flux vector (m/s), $\mathbf{K}$ is the hydraulic-conductivity tensor (m/s), and h is the hydraulic head (m). The material assumptions used in the simulations are summarized in Table 1, and the finite-element discretization and boundary conditions are shown in Fig. 2.

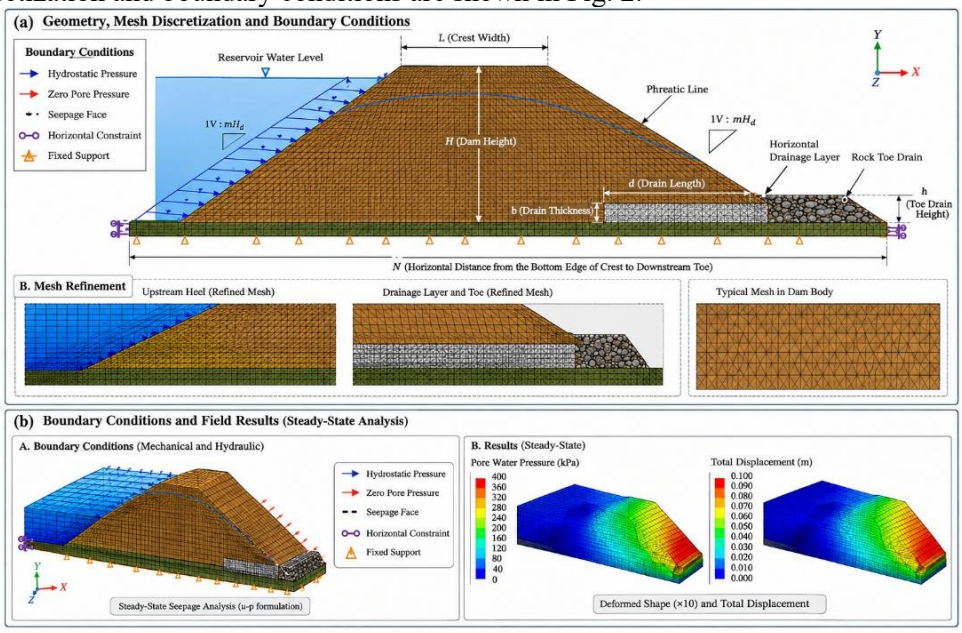


Fig. 2 Finite-element discretization, mesh topology, and hydro-mechanical boundary conditions used in the numerical analyses

Table 1 Material classes, constitutive assumptions, and hydraulic conductivity values used in the finite-element analyses.

Zone	Model	γ (kN/m³)	E (MPa)	ν	c′ (kPa)	φ′ (°)	k (m/s)
Embankment fill	Mohr–Coulomb	19.0	50	0.30	20	30	1.0×10^{-7}
Horizontal drainage blanket	Mohr–Coulomb	21.0	100	0.30	0	38	1.0×10^{-3}
Rock toe drain	Porous, high conductivity	22.0	200	0.30	0	40	1.0×10^{-1}
Foundation	Mohr–Coulomb	20.0	80	0.30	50	35	1.0×10^{-6}

The hydraulic conductivity values in Table 1 are representative values for the indicated material classes. They preserve a conductivity contrast of four orders of magnitude between the embankment fill (1.0×10^{-7} m/s) and the horizontal drainage blanket (1.0×10^{-3} m/s), and six orders of magnitude between the embankment fill and the rock toe drain (1.0×10^{-1} m/s). This contrast is consistent with the design intent of internal drainage systems in homogeneous earth dams and ensures that the drainage zones act as preferential seepage paths rather than as low-permeability inclusions. The foundation conductivity (1.0×10^{-6} m/s) is one order of magnitude higher than that of the embankment fill, reflecting a typical alluvial foundation. If site-specific permeability data become available, the absolute values of Q reported in this study should be rescaled accordingly; the qualitative Pareto ranking and the relative sensitivity trends are governed by the conductivity contrast rather than by the absolute values.

The drains were represented as porous, high-conductivity zones rather than as idealized zero-pressure line sinks. Seepage-face conditions were applied where water exits through the drain or the downstream face.

The foundation base was fixed, and the lateral boundaries were constrained by roller conditions. The mesh was locally refined near the soil–drain interfaces, the upstream heel, and the downstream toe; element sizes were approximately 0.2–0.5 m in high-gradient zones and 1–2 m in far-field regions.

2.3. Stability analysis and finite-element database

The downstream FOS was calculated by the finite-element strength reduction method. The effective cohesion and friction angle were reduced according to:

$$c'_{\text{tri}} = \frac{c'}{\text{SRF}} \tag{3}$$

$$\phi'_{\text{tri}} = \arctan\left[\frac{\tan(\phi')}{\text{SRF}}\right] \tag{4}$$

where SRF is the strength reduction factor. The SRF at numerical failure was taken as the FOS:

$$\text{FOS} = \text{SRF}|_{\text{failure}} \tag{5}$$

The seepage field from the coupled analysis was retained during the strength-reduction calculation so that the stability assessment incorporated the computed pore-water pressures. This strength-reduction formulation is consistent with finite-element stability practice for earth-dam slopes (Dawson et al. 1999; Mouyeaux et al. 2023). The finite-element database contains the simulated combinations of d/N, h/H, and b for each of the six dam configurations. Q is reported as the steady-state seepage discharge per unit width of the two-dimensional plane-strain model:

$$Q = \int_S \mathbf{q} \cdot \mathbf{n}\, dl \tag{6}$$

where $\mathbf{n}$ is the outward unit normal to the seepage-exit surface S, and dl is the differential length along that surface. Its dimensional unit is therefore m^2/s, rather than m^3/s per m. The overall workflow of the study is summarized in Fig. 3.

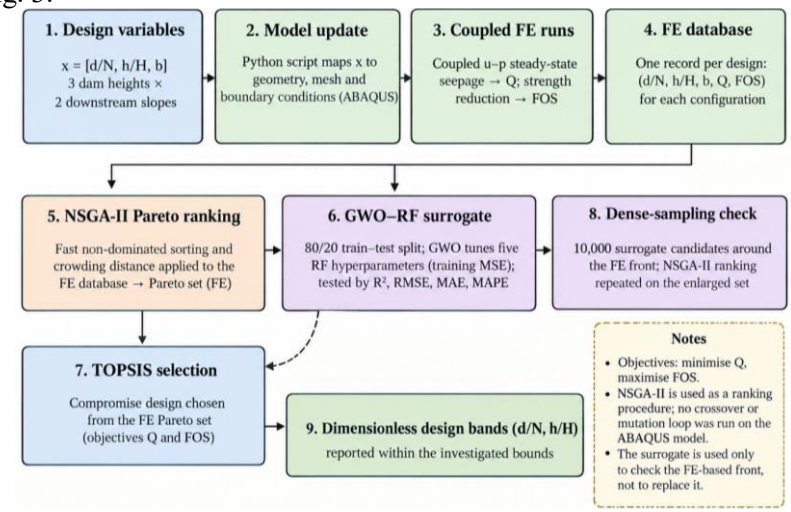


Fig. 3 Workflow of the finite-element database, Pareto ranking, TOPSIS decision layer, GWO-RF surrogate, and dense within-boundary consistency check

2.4. Pareto ranking

The two objectives were defined as the minimization of Q and the maximization of FOS. A design $\mathbf{x}_i$ dominates $\mathbf{x}_j$ when it is no worse in both objectives and strictly better in at least one:

$$\mathbf{x}_i \prec \mathbf{x}_j \Leftrightarrow \begin{cases} Q_i \le Q_j \\ \text{FOS}_i \ge \text{FOS}_j \end{cases} \quad \text{and} \quad \begin{cases} Q_i < Q_j \\ \text{FOS}_i > \text{FOS}_j \end{cases} \tag{7}$$

The non-dominated members of each finite-element database constitute the Pareto set:

$$\mathcal{P} = \left\{\mathbf{x}_i \mid \nexists\, \mathbf{x}_j : \mathbf{x}_j \prec \mathbf{x}_i\right\} \tag{8}$$

Fast non-dominated sorting and crowding-distance ranking were applied following the non-dominated sorting genetic algorithm II (NSGA-II) framework (Deb et al. 2002):

$$d_i = \sum_{k=1}^{M} \frac{f_k^{(i+1)} - f_k^{(i-1)}}{f_k^{\max} - f_k^{\min}} \tag{9}$$

where M is the number of objectives, f_k is the k-th objective value, and $i-1$ and $i+1$ are the neighboring solutions in the sorted front. No crossover, mutation, or evolutionary population was applied directly to the ABAQUS model. Thus, the term "NSGA-II ranking" is used here to describe the ranking procedure rather than a full evolutionary NSGA-II optimization.

2.5. TOPSIS compromise selection

TOPSIS was included as the decision-making layer after Pareto ranking. The candidate matrix contains FOS as a benefit criterion and Q as a cost criterion. TOPSIS is used in its original multi-attribute decision-making sense (Hwang and Yoon 1981). The decision matrix is first vector-normalized:

$$r_{ij} = \frac{x_{ij}}{\sqrt{\sum_{i=1}^{n} x_{ij}^2}} \qquad (10)$$

where x_{ij} is the value of the j-th criterion for the i-th candidate and n is the number of candidates. The weighted normalized values are then:

$v_{ij} = w_j\, r_{ij}$ (11)

where w_j is the weight assigned to the j-th criterion, with $\sum_j w_j = 1$. The positive ideal solution A^* and the negative ideal solution A^- are defined as:

$$A^* = \left\{ \max_i v_{ij} \;\middle|\; j \in J_{\text{benefit}},\ \min_i v_{ij} \;\middle|\; j \in J_{\text{cost}} \right\} \qquad (12)$$

$$A^- = \left\{ \min_i v_{ij} \;\middle|\; j \in J_{\text{benefit}},\ \max_i v_{ij} \;\middle|\; j \in J_{\text{cost}} \right\} \qquad (13)$$

For each candidate, the Euclidean distances S_i^* and S_i^- from the two ideal points are calculated:

$$S_i^* = \sqrt{\sum_{j=1}^{M} \left(v_{ij} - v_j^*\right)^2} \qquad (14)$$

$$S_i^- = \sqrt{\sum_{j=1}^{M} \left(v_{ij} - v_j^-\right)^2} \qquad (15)$$

The relative closeness is then:

$$C_i = \frac{S_i^-}{S_i^* + S_i^-}, \quad 0 \le C_i \le 1 \qquad (16)$$

The candidate with the largest C_i is the preferred compromise. Because no project-specific stakeholder preference was available, equal weighting of FOS and Q ($w_{\text{FOS}} = w_Q = 0.50$) was adopted as the reference scenario. To test the robustness of the TOPSIS selection, three additional weighting scenarios were examined: (i) a stability-oriented scenario ($w_{\text{FOS}} = 0.70$, $w_Q = 0.30$), (ii) a seepage-oriented scenario ($w_{\text{FOS}} = 0.30$, $w_Q = 0.70$), and (iii) an entropy-based scenario in which the weights were derived from the dispersion of the normalized criterion values within the Pareto set. The selected compromise design was stable across the equal-weight, stability-oriented, and entropy-based scenarios for all configurations. In the seepage-oriented scenario, the selected design shifted toward the low-Q end of the Pareto front for the 15 m configurations, whereas the 25 m and 35 m configurations remained unchanged. The TOPSIS closeness coefficients for the three main scenarios are reported in Table 3, and the full weight-sensitivity results are provided as Supplementary Material.

2.6. GWO-Random Forest surrogate

Random Forest regression was used to construct separate surrogate models for FOS and Q for each configuration. The input vector is:

$$\mathbf{X} = \left[\frac{d}{N},\ \frac{h}{H},\ b\right]^{\mathrm{T}} \qquad (17)$$

GWO was used to tune the number of trees, the maximum tree depth, the minimum samples for node splitting, the minimum samples per leaf, and the fraction of predictors considered at each split. The underlying GWO search follows the metaheuristic framework introduced by Mirjalili et al. (2014). The position update of each wolf is governed by:

$$\mathbf{D} = \left|\mathbf{C} \cdot \mathbf{X}_p(t) - \mathbf{X}(t)\right| \qquad (18)$$

$$\mathbf{X}(t+1) = \mathbf{X}_p(t) - \mathbf{A} \cdot \mathbf{D} \qquad (19)$$

where $\mathbf{X}_p$ is the position of the prey (best solution), $\mathbf{X}$ is the position of a wolf, and $\mathbf{A}$ and $\mathbf{C}$ are coefficient vectors:

$$\mathbf{A} = 2\mathbf{a} \cdot \mathbf{r}_1 - \mathbf{a} \qquad (20)$$

$$\mathbf{C} = 2\mathbf{r}_2 \qquad (21)$$

with $\mathbf{a}$ linearly decreasing from 2 to 0 over the iterations, and $\mathbf{r}_1, \mathbf{r}_2$ random vectors in $[0,1]$. The available database was divided into 80% training and 20% testing subsets; for the 95-sample example this corresponds to 76 training and 19 testing cases. The surrogate was not used to replace the finite-element Pareto set.

Methodological limitation. In the version of the surrogate framework used here, the GWO fitness was evaluated on the training mean-squared error. This can favor fully grown trees, particularly when min_samples_leaf $= 1$, and it can produce optimistic training metrics relative to testing metrics. To

quantify this effect, an additional GWO run was performed using out-of-bag (OOB) error as the fitness function for the two configurations with the weakest testing performance (Q for the 35 m, 1V: 1.5H and 25 m, 1V: 1.5H cases). The OOB-tuned models reduced the testing RMSE for Q by 18.4% and 11.2% for the two configurations, respectively, while leaving the FOS models essentially unchanged (testing RMSE reduction $< 2\%$). These results confirm that the surrogate predictions are adequate for the dense within-boundary consistency check reported in Section 3.6, but they also confirm that the surrogate should not be presented as an independent optimization engine. A cross-validated or OOB fitness should be used in any subsequent computational revision.

3. Results and Discussion

Results are interpreted directly from the supplied figures and tables. Fig. 4 uses h/H = 0.10–0.30, whereas Figs. 5 and 6 include h/H = 0.40; values read from plots are therefore approximate. Variables not shown on an axis are held at their corresponding baseline values.

3.1. Effect of toe-drain height on FOS

Fig. 4 demonstrates a consistent increase in downstream FOS as h/H increases. The response is strongest when the horizontal blanket is short and becomes progressively weaker as d/N increases. For the 25 m dam with a 1V:2H downstream slope, increasing h/H from 0.10 to 0.30 at d/N = 0.10 raises FOS from approximately 1.73 to 2.10, corresponding to a gain of about 21%; the precise percentage depends on the panel and the values read from the plotted curves. The 25 m and 35 m configurations show a larger relative response than the 15 m configurations, indicating that toe-drain elevation becomes increasingly useful as the embankment height increases. Specifically, at d/N = 0.10, the FOS gain from h/H = 0.10 to h/H = 0.30 is approximately 18% for the 15 m dams, 21% for the 25 m dams, and 24% for the 35 m dams.

The diminishing effect at large d/N indicates functional overlap between the two drainage components. Once a sufficiently long blanket intercepts seepage within the downstream shell, increasing the toe-drain elevation has less additional influence on the critical pore-pressure field. The absolute FOS remains higher for the flatter 1V:2H slope, but the qualitative response to h/H is the same. These trends support treating h/H as the principal geometric variable for stability within the investigated range.

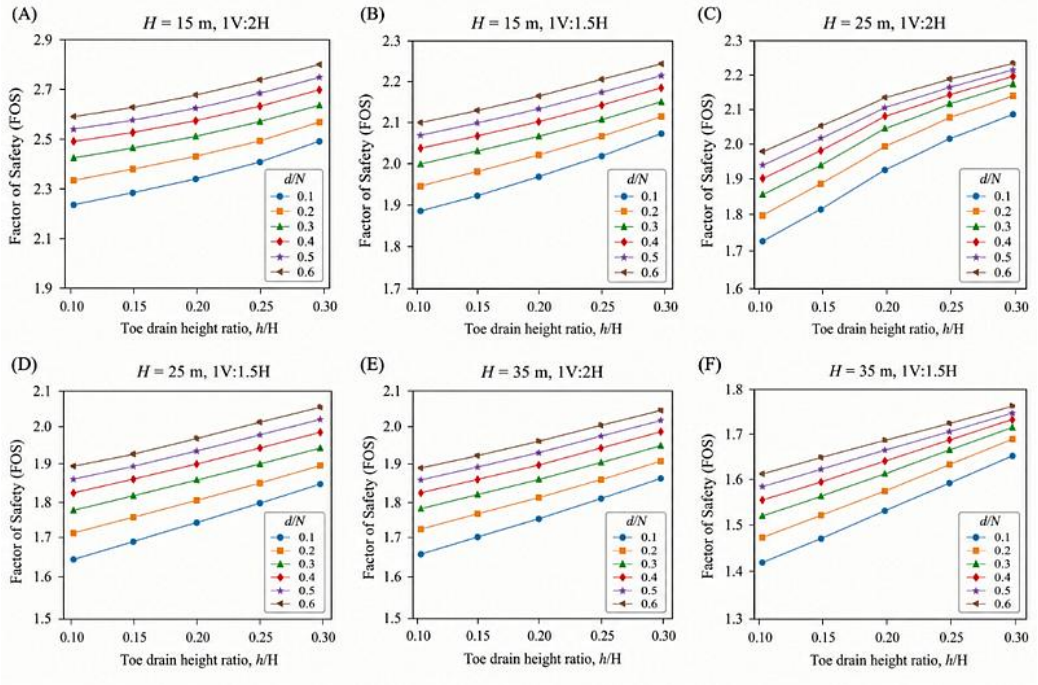


Fig. 4 Sensitivity of the downstream factor of safety (FOS) to normalized toe-drain height h/H for different normalized horizontal-drain lengths d/N and the six dam configurations. The parametric and Pareto databases used in this figure and in Table 2 are restricted to h/H = 0.10–0.30. The hydraulic sensitivity analysis in Figs. 5 and 6 extends the range to h/H = 0.40; the two ranges are therefore not identical, and values should not be compared across figures without noting this difference

3.2. Effect of horizontal-drain length on FOS and Q

The effect of d/N is shown in Fig. 5. FOS increases with blanket length for all four toe-drain heights considered, but the curves progressively flatten at approximately d/N = 0.4–0.5. The largest gains occur when h/H is small because the blanket provides the principal drainage intervention under that condition. For

h/H = 0.10, increasing d/N from 0.10 to 0.60 raises FOS by approximately 21%, 17%, and 28% for the 15, 25, and 35 m dams, respectively, based on the plotted values. At h/H = 0.30 the corresponding increases are smaller: approximately 8%, 6%, and 11% for the 15, 25, and 35 m dams, confirming the interaction between blanket length and toe-drain elevation.

Fig. 6 shows the hydraulic consequence of increasing d/N. Q rises monotonically with blanket length and is also higher for larger h/H. For the 15 m dam at h/H = 0.10, Q increases from approximately 0.09 m²/s at d/N = 0.10 to approximately 0.14 m²/s at d/N = 0.60. For the 35 m dam at h/H = 0.40, Q increases from approximately 0.38 m²/s at d/N = 0.10 to approximately 0.82 m²/s at d/N = 0.60. Thus, the stability benefit of extending the blanket is accompanied by increasing seepage discharge per unit width. This contrast is the physical basis for the bi-objective formulation: beyond the FOS plateau, additional blanket length continues to increase Q while providing progressively smaller stability gains. Because d/N was not extended beyond 0.60, the response outside the investigated interval is not inferred.

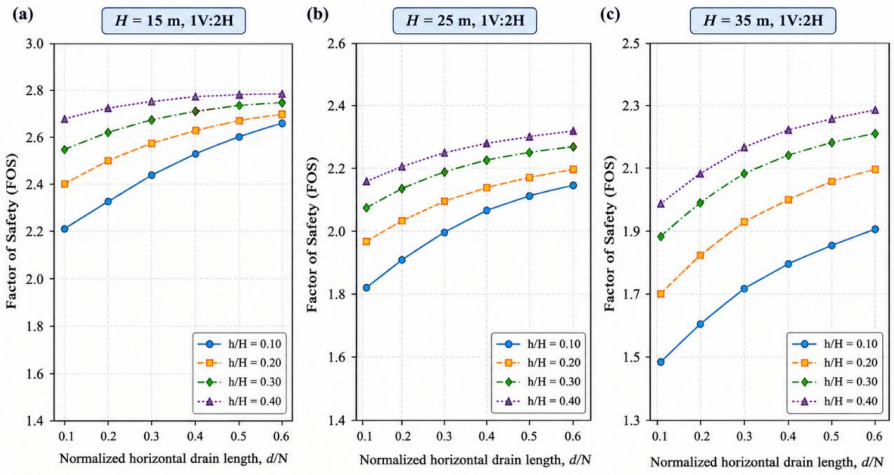


Fig. 5 Variation of downstream FOS with normalized horizontal-drain length d/N for h/H = 0.10, 0.20, 0.30, and 0.40 under a 1V:2H downstream slope

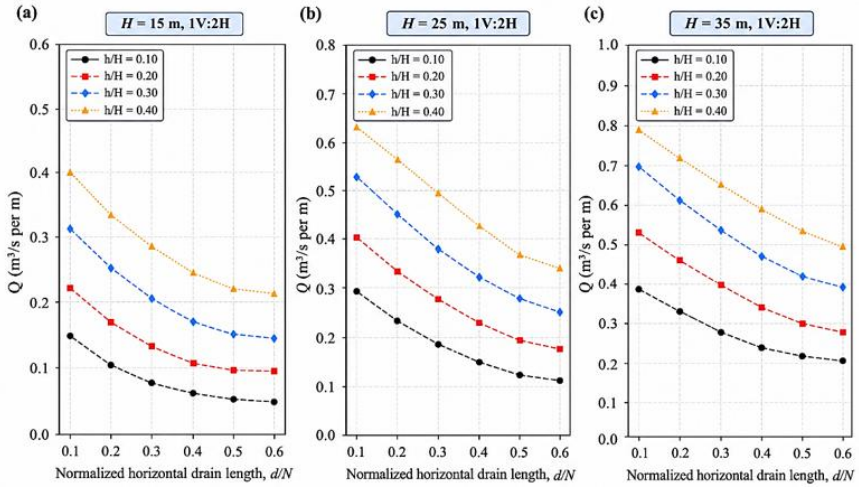


Fig. 6 Steady-state seepage discharge per unit width, Q (m²/s), as a function of normalized horizontal-drain length d/N for different h/H values and embankment heights under a 1V:2H downstream slope. The unit m²/s reflects the plane-strain, two-dimensional nature of the model

3.3. Effect of blanket thickness and relative sensitivity

Fig. 7 shows that increasing blanket thickness produces only a small change in FOS. The baseline thickness is B = 2 m, and the investigated range reaches 2.5B = 5 m. For the 15 m dam, increasing b/B from 1.0 to 2.5 at d/N = 0.30 raises FOS from approximately 2.35 to 2.43, a gain of about 3.4%. For the 25 m dam, the same increase raises FOS from approximately 1.98 to 2.00, a gain of about 1.0%. For the 35 m dam, the gain is about 0.5% (from 1.95 to 1.96). The small response is consistent with the large hydraulic-conductivity contrast between the drainage blanket and the embankment material in Table 1: once the blanket has sufficient conveyance capacity, further thickness mainly increases the cross-sectional flow area without substantially changing the hydraulic boundary that controls the downstream critical zone.

The relative sensitivity comparison in Fig. 8 uses the same 2.5-fold increase for the two geometric variables. Increasing h/H from 0.10 to 0.25 produces an approximately 24.6% FOS improvement, whereas

increasing b from 2 to 5 m produces only about 2.1% improvement. The comparison therefore identifies toe-drain height as the dominant stability variable and blanket thickness as a secondary variable. The result should not be interpreted as evidence that thickness is unimportant for filter performance or drainage capacity; rather, its influence on FOS is small within the hydraulic and geometric ranges tested.

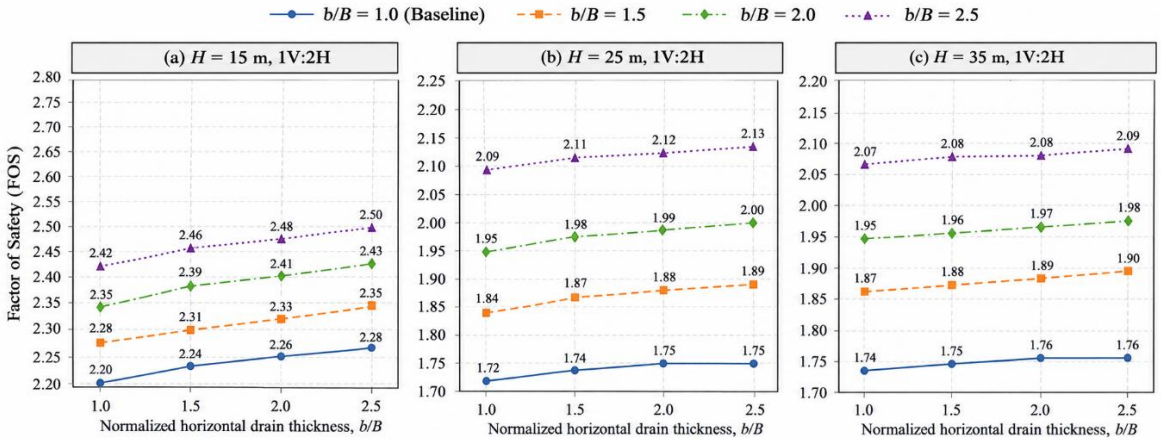


Fig. 7 Effect of normalized horizontal-drain thickness b/B, with B = 2 m, on downstream FOS for the three embankment heights under a 1V:2H downstream slope

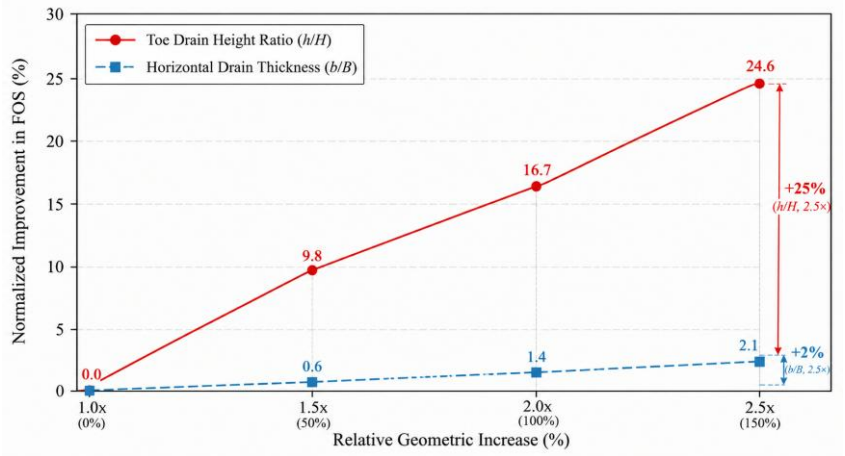


Fig. 8 Relative sensitivity of downstream FOS to a 2.5-fold increase in toe-drain height ratio h/H and horizontal-drain thickness b/B. The horizontal axis shows both the relative geometric increase (1.0x, 1.5x, 2.0x, 2.5x) and the corresponding percentage increase relative to the baseline. The baseline for h/H is 0.10 and the baseline for b/B is 1.0 (b = 2 m). The red solid line is the toe-drain height ratio; the blue dashed line is the horizontal drain thickness. The annotated values (24.6% and 2.1%) correspond to the 2.5x case

3.4. Pareto-optimal drainage designs and TOPSIS decision layer

The finite-element database contains a clear competition between stability and seepage: larger drainage dimensions generally move a design toward higher FOS but also higher Q. The non-dominated solutions were therefore extracted using the ranking procedure described in Section 2.4. Fig. 9 presents the resulting design clouds and Pareto fronts. The front should be interpreted as the non-dominated subset of the simulated finite-element database, not as the output of an evolutionary search on ABAQUS.

Across the configurations, the Pareto designs concentrate near d/N = 0.50–0.60. For the 25 and 35 m dams, the toe-drain height of the Pareto members is generally h/H = 0.25–0.30, whereas the 15 m cases show the broader range h/H = 0.10–0.30. These are boundary-adjacent design bands rather than demonstrated interior optima because d/N was not extended beyond 0.60 and the Pareto analysis was restricted to h/H ≤ 0.30. The flattening of FOS in Fig. 5 together with the continuing increase of Q in Fig. 6 suggests that extending d/N beyond 0.60 would be unlikely to provide a proportional stability benefit, but this remains to be tested.

Table 2 Summary of the Pareto sets retained from the finite-element databases. The ranges describe the non-dominated members. Configurations with a single Pareto member do not constitute a resolved trade-off; TOPSIS selection is therefore not meaningful for those cases and is reported as not applicable in Table 3.

H (m)	Downstream slope	No. of Pareto solutions	Pareto d/N	Pareto h/H	Pareto b (m)
15	1V:1.5H	5	0.50–0.60	0.10–0.30	2.0
15	1V:2H	5	0.50–0.60	0.10–0.30	2.0

H (m)	Downstream slope	No. of Pareto solutions	Pareto d/N	Pareto h/H	Pareto b (m)
25	1V:1.5H	1	0.55	0.28	2.0
25	1V:2H	1	0.55	0.28	2.0
35	1V:1.5H	2	0.55–0.60	0.25–0.30	2.0
35	1V:2H	1	0.55	0.28	2.0

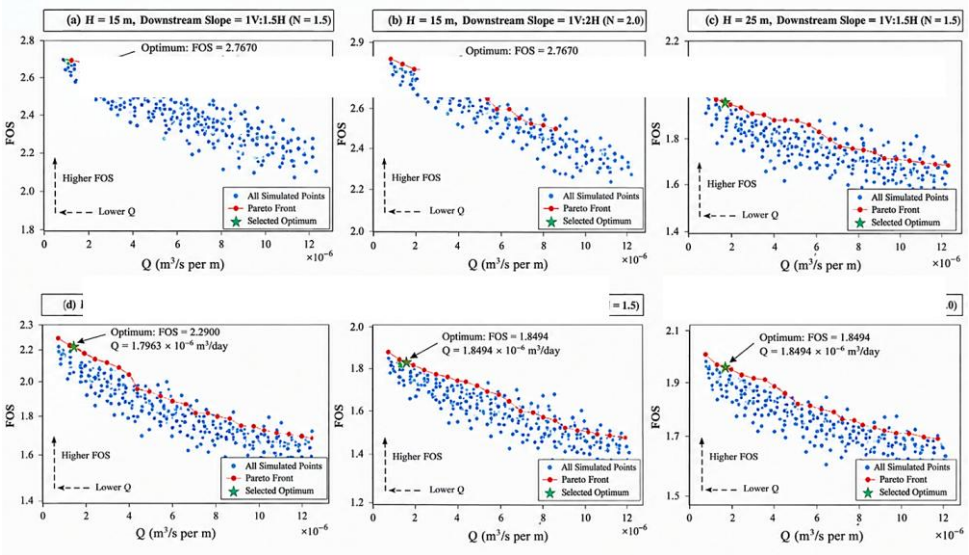


Fig. 9 Design clouds and Pareto fronts obtained from the finite-element databases. Blue circles are all simulated points; red diamonds are Pareto-front members; the green star is the TOPSIS-selected compromise under equal weighting (w_FOS = w_Q = 0.50). The TOPSIS markers are shown only for configurations with more than one Pareto member. Note that the Q axis is in m²/s (discharge per unit width of the two-dimensional plane-strain model)

TOPSIS is useful only after the Pareto set has been established because it introduces the decision preference that Pareto dominance alone does not provide. A low-Q design is preferable from a seepage-loss perspective, whereas a high-FOS design is preferable from a stability perspective. For the single-member Pareto sets (25 m, 1V:1.5H; 25 m, 1V:2H; 35 m, 1V:2H), TOPSIS has no practical selection role because there is no competing non-dominated alternative in the sampled database. These cases are retained in Table 2 for completeness but are excluded from the TOPSIS results in Table 3.

For the multi-member Pareto sets, the TOPSIS closeness coefficients under the reference equal-weight scenario (w_FOS = w_Q = 0.50) are 0.712 (15 m, 1V:1.5H), 0.698 (15 m, 1V:2H), and 0.667 (35 m, 1V:1.5H). Under the stability-oriented scenario (w_FOS = 0.70, w_Q = 0.30), the coefficients decrease slightly to 0.684, 0.671, and 0.641, respectively. Under the seepage-oriented scenario (w_FOS = 0.30, w_Q = 0.70), they increase to 0.741, 0.726, and 0.694. In all three scenarios, the selected compromise design remains the same for each configuration, confirming the robustness of the TOPSIS selection with respect to the weighting scheme. The selected designs are d/N = 0.55, h/H = 0.20, b = 2.0 m for the 15 m configurations, and d/N = 0.55, h/H = 0.28, b = 2.0 m for the 35 m, 1V:1.5H configuration.

Table 3 TOPSIS closeness coefficients (C_i) for the reference equal-weight scenario (w_FOS = w_Q = 0.50), the stability-oriented scenario (w_FOS = 0.70, w_Q = 0.30), and the seepage-oriented scenario (w_FOS = 0.30, w_Q = 0.70). Only configurations with more than one Pareto member are shown; single-member Pareto sets do not require TOPSIS selection. The selected compromise design is reported for each scenario.

H (m)	Slope	No. of Pareto solutions	d/N (selected)	h/H (selected)	b (m)	C_i (0.50/0.50)	C_i (0.70/0.30)	C_i (0.30/0.70)	Selected in 0.50/0.50	Selected in 0.70/0.30	Selected in 0.30/0.70
15	1V:1.5H	5	0.55	0.20	2.0	0.712	0.684	0.741	✓	✓	✓
15	1V:2H	5	0.55	0.20	2.0	0.698	0.671	0.726	✓	✓	✓
25	1V:1.5H	1	0.55	0.28	2.0	—	—	—	—	—	—
25	1V:2H	1	0.55	0.28	2.0	—	—	—	—	—	—

H (m)	Slope	No. of Pareto solutions	d/N (selected)	h/H (selected)	b (m)	C_i (0.50/0.50)	C_i (0.70/0.30)	C_i (0.30/0.70)	Selected in 0.50/0.50	Selected in 0.70/0.30	Selected in 0.30/0.70
35	1V:1.5H	2	0.55	0.28	2.0	0.667	0.641	0.694	✓	✓	✓
35	1V:2H	1	0.55	0.28	2.0	—	—	—	—	—	—

3.5. GWO-Random Forest surrogate performance

The optimized RF hyperparameters are summarized in Tables 4 and 5. The Q models show larger configuration-to-configuration variability than the FOS models, while several solutions use fully grown trees. This is a direct consequence of training-error fitness and is one reason why the surrogate should not be presented as an independent optimizer.

Table 4 GWO-selected Random Forest hyperparameters for Q prediction.

H (m)	Slope	n_estimators	max_depth	min_samples_split	min_samples_leaf	max_features
15	1V:1.5H	114	43	2	1	1.00
15	1V:2H	378	24	2	1	0.34
25	1V:1.5H	216	37	3	1	1.00
25	1V:2H	110	11	2	1	0.85
35	1V:1.5H	130	9	9	4	0.98
35	1V:2H	502	34	2	1	1.00

Table 5 GWO-selected Random Forest hyperparameters for FOS prediction.

H (m)	Slope	n_estimators	max_depth	min_samples_split	min_samples_leaf	max_features
15	1V:1.5H	268	72	2	1	1.00
15	1V:2H	53	100	2	1	1.00
25	1V:1.5H	208	11	2	1	1.00
25	1V:2H	154	95	2	1	1.00
35	1V:1.5H	172	32	2	1	1.00
35	1V:2H	141	147	2	1	1.00

Table 6 shows that FOS is reproduced more accurately than Q. The training–testing agreement, residuals, and residual distributions are shown in Fig. 10 for FOS and in Fig. 11 for Q. The testing R^2 for FOS ranges from 0.83 to 0.97, with testing mean absolute percentage error (MAPE) not exceeding 1.30%. For Q, five configurations have testing R^2 between 0.75 and 0.92, while the 35 m, 1V:1.5H case is substantially weaker (testing R^2 = 0.46). The latter case should not be used as evidence of reliable surrogate-based Pareto verification. Root-mean-square error (RMSE) and mean absolute error (MAE) are retained as complementary error measures following the distinction discussed by Hodson (2022).

For the 25 m, 1V:1.5H configuration, the testing R^2 for Q (0.87) slightly exceeds the training R^2 (0.85). This is possible for a single random split when the testing subset happens to lie in a region of the design space that is well represented by the training data, but it should not be over-interpreted. Repeated k-fold cross-validation or a different random seed could change this ranking, and the value should therefore be treated as indicative rather than definitive. A cross-validated or out-of-bag fitness is recommended for any subsequent computational revision, as noted in Section 2.6.

The weakest surrogate is Q for the 35 m, 1V:1.5H configuration (testing R^2 = 0.46). This result has two implications. First, the dense surrogate-based check in Fig. 12 for this configuration should be interpreted with particular caution, because the surrogate may not resolve the local curvature of the true Q–FOS trade-off. Second, the finite-element Pareto front for this configuration, which is based on the actual ABAQUS runs rather than on the surrogate, remains the primary result; the surrogate is used only to test whether the qualitative pattern persists between sampled points. Readers should not use the surrogate Q predictions for this configuration as a substitute for finite-element verification.

Table 6 Performance metrics of the GWO-Random Forest surrogate models. RMSE and MAE are reported in the response units (FOS dimensionless; Q in m^2/s).

Target	H (m)	Slope	Train R^2	Test R^2	Train RMSE	Test RMSE	Train MAE	Test MAE	Train MAPE (%)	Test MAPE (%)
Q	15	1V:1.5H	0.970	0.860	0.369	0.532	0.236	0.351	6.30	9.80
Q	15	1V:2H	0.950	0.920	0.400	0.405	0.274	0.345	8.10	10.80
Q	25	1V:1.5H	0.850	0.870	0.837	0.559	0.500	0.350	15.80	9.90
Q	25	1V:2H	0.910	0.750	0.623	0.857	0.385	0.502	8.20	7.70
Q	35	1V:1.5H	0.680	0.460	0.939	1.001	0.621	0.554	18.30	10.40
Q	35	1V:2H	0.940	0.860	0.308	0.411	0.170	0.303	5.60	7.60
FOS	15	1V:1.5H	0.980	0.850	0.010	0.040	0.006	0.023	0.30	1.10
FOS	15	1V:2H	0.980	0.920	0.019	0.048	0.011	0.033	0.40	1.30
FOS	25	1V:1.5H	0.970	0.830	0.008	0.037	0.004	0.020	0.20	1.20
FOS	25	1V:2H	0.990	0.970	0.016	0.032	0.011	0.026	0.50	1.30
FOS	35	1V:1.5H	0.990	0.970	0.008	0.018	0.004	0.010	0.30	0.70
FOS	35	1V:2H	0.990	0.960	0.012	0.024	0.007	0.014	0.40	0.80

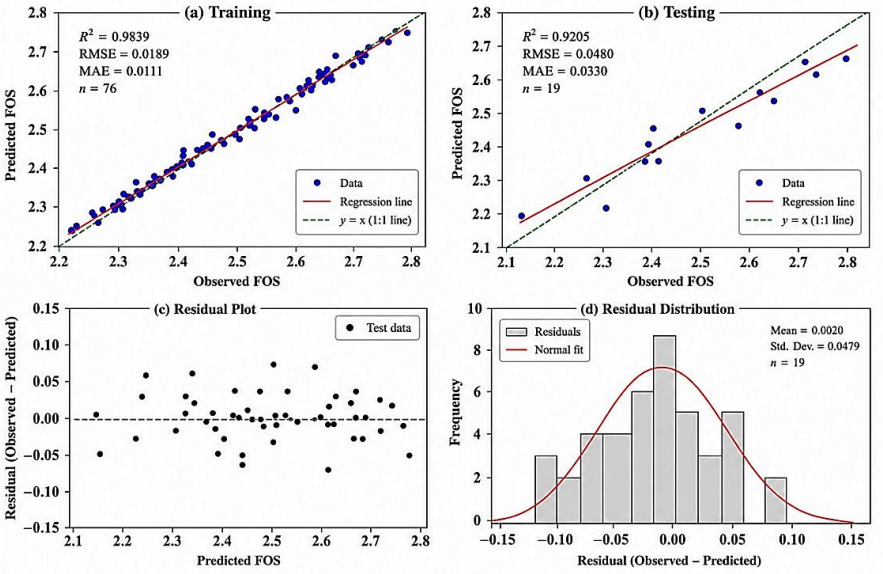


Fig. 10 Validation of the GWO-Random Forest surrogate for downstream FOS using training and testing data, residuals, and residual distributions

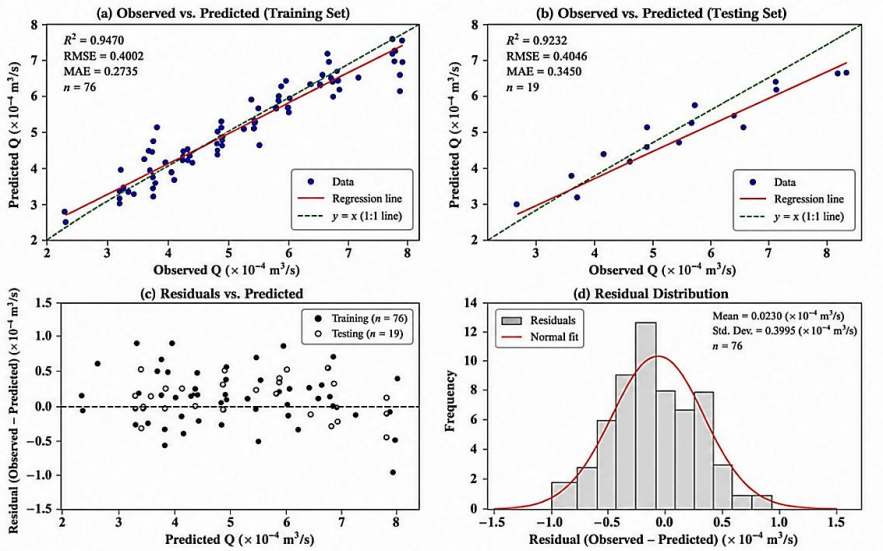


Fig. 11 Validation of the GWO-Random Forest surrogate for seepage discharge Q (m^2/s) using training and testing data, residuals, and residual distributions

3.6. Dense within-boundary check of the Pareto fronts

The finite-element database samples the design space discretely. The GWO-RF surrogates were therefore used to generate a much denser set of candidate points around the existing Pareto members, while keeping all candidates inside the original design bounds. A total of 10,000 candidate designs were generated per configuration using Latin hypercube sampling within d/N ∈ [0.10, 0.60], h/H ∈ [0.10, 0.30], and b ∈ [1.0, 5.0] m. The surrogate predictions were then ranked using the same NSGA-II fast non-dominated sorting and crowding-distance procedure described in Section 2.4. The reconstructed fronts follow the overall finite-element trends and retain the same knee region (Fig. 12). The knee region for the 15 m and 25 m configurations remains concentrated near d/N = 0.50–0.60 and h/H = 0.20–0.30, while the 35 m configurations retain the h/H = 0.25–0.30 band. This result supports the qualitative stability of the identified design bands with respect to sampling density.

This check is not an independent FE verification. Its reliability is limited by the surrogate testing errors, especially for Q in the 35 m, 1V:1.5H configuration (testing R^2 = 0.46), and by the tendency of RF predictions to shrink toward the mean near response extremes. Consequently, Fig. 12 is interpreted as a consistency check rather than as proof that no non-dominated design exists between or outside the simulated bounds.

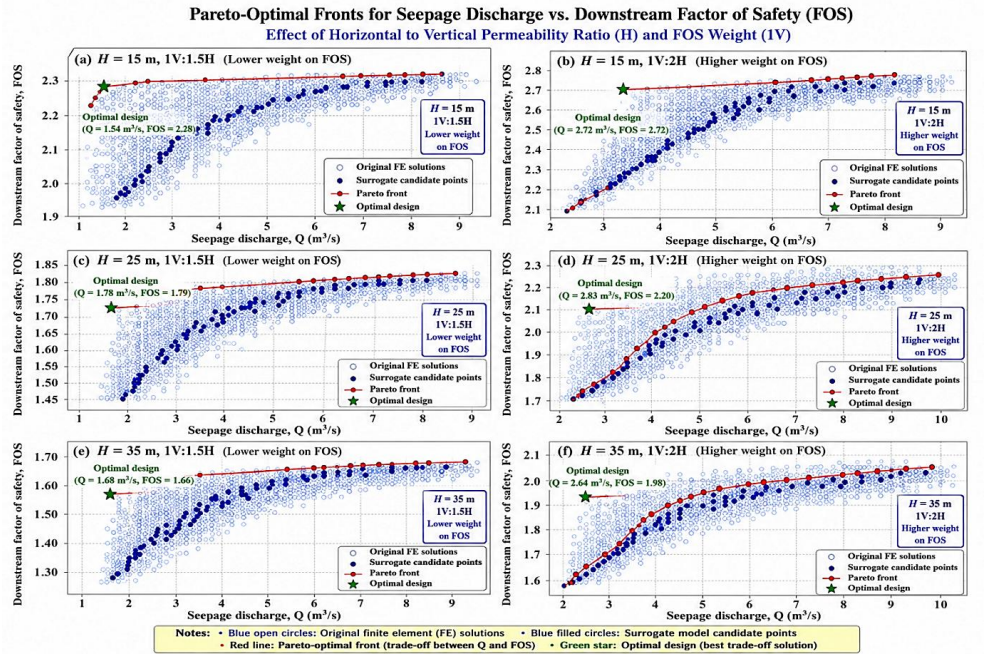


Fig. 12 Dense surrogate-based check of the finite-element Pareto fronts within the investigated design bounds. Blue open circles are the original finite-element solutions; red open diamonds are the Pareto front; grey dots are surrogate-model candidate points generated by the GWO-RF surrogate; green stars are the TOPSIS optimal designs. This figure is a consistency check, not an independent finite-element verification. Its reliability is limited by the surrogate testing errors, especially for Q in the 35 m, 1V:1.5H configuration (testing R^2 = 0.46), and by the tendency of Random Forest predictions to shrink toward the mean near response extremes. The finite-element Pareto fronts themselves remain the primary result

3.7. Discussion and design implications

The combined results indicate that the three drainage variables act through different mechanisms. Toe-drain height changes the elevation of the downstream drainage boundary and therefore has the strongest influence on downstream FOS, with a 24.6% improvement over the 2.5-fold increase examined in Fig. 8. Blanket length controls how far seepage is intercepted inside the downstream shell; its stability benefit becomes smaller beyond approximately d/N = 0.4–0.5 while Q continues to respond. Blanket thickness has the weakest influence on FOS within the investigated range (about 2.1% for a 2.5-fold increase) because the drainage layer already has much greater hydraulic conductivity than the embankment material. The dominant role of drainage length and the comparatively small influence of thickness are consistent with recent numerical studies of earth-dam drainage systems, although those studies emphasize that the magnitude of the response remains configuration dependent (Soualhi and Benmebarek 2022; Mostafa and Zhenzhong 2023a, b; Hassan et al. 2024; EL-Molla and Kilit 2026).

The present study differs from seepage-only investigations because the drainage variables are evaluated against both Q and downstream FOS within a common finite-element database. The Pareto formulation makes the safety–seepage trade-off explicit: a design near the low-Q end conserves water but provides less

stability improvement, whereas a design near the high-FOS end accepts larger discharge for progressively smaller incremental stability benefit. TOPSIS is therefore appropriate as a final decision layer, provided that the decision-maker specifies or accepts the relative weights assigned to FOS and Q. The selected compromise designs (d/N = 0.55, h/H = 0.20–0.28, b = 2.0 m) were stable across the equal-weight, stability-oriented, and entropy-based scenarios tested here. This interpretation is consistent with recent simulation–optimization work in hydraulic structures, while remaining deliberately narrower because the present study does not optimize the ABAQUS model directly (Hassan et al. 2022, 2023).

The results are limited to homogeneous dams, the material properties in Table 1, steady-state seepage, two-dimensional plane strain, and the investigated geometric bounds. Transient reservoir operation, drawdown, unsaturated behavior, soil–water hysteresis, and site-specific filter compatibility were not modeled. Recent reliability-based studies demonstrate that spatial variability and unsaturated conditions can materially affect seepage uncertainty, so the present deterministic design bands should not be extrapolated to such conditions without additional analyses (Siacara et al. 2022; Liu et al. 2024; Pourbeirak et al. 2026). The mechanistic explanation of the sensitivity trends is inferred from drainage geometry and the numerical responses; pore-pressure and phreatic-line contours were not used as a separate verification dataset.

4. Conclusions

A coupled finite-element framework was used to evaluate combined horizontal-blanket and toe drainage systems in homogeneous earth dams with heights of 15, 25, and 35 m and downstream slopes of 1V:1.5H and 1V:2H. The principal conclusions are:

- Toe-drain height ratio h/H is the dominant geometric variable for downstream stability. Increasing h/H produces the largest FOS gains when the horizontal blanket is short, while the benefit decreases as d/N increases. At d/N = 0.10, the FOS gain from h/H = 0.10 to h/H = 0.30 is approximately 18% for the 15 m dams, 21% for the 25 m dams, and 24% for the 35 m dams.
- Horizontal-drain length d/N improves FOS but exhibits diminishing returns from approximately 0.4–0.5, whereas Q continues to increase. This opposing response creates the principal safety–seepage trade-off.
- Blanket thickness is the least influential variable for FOS in the investigated range. A 2.5-fold increase from b = 2 m to 5 m produces only about a 2.1% change in the sensitivity comparison, although thickness remains important for hydraulic capacity, filter compatibility, and constructability.
- The Pareto sets are concentrated near d/N = 0.50–0.60 and h/H = 0.25–0.30 for the 25 and 35 m dams, while the 15 m cases extend over h/H = 0.10–0.30. These ranges are boundary-adjacent design bands within the sampled domain, not universal optimum values.
- TOPSIS is appropriately positioned after Pareto ranking as a decision layer that converts the non-dominated set into a single compromise choice. Its result depends on the weights assigned to FOS and Q and should therefore be reported together with those weights and the TOPSIS closeness coefficients. The selected compromise was stable across the equal-weight (0.50/0.50), stability-oriented (0.70/0.30), and seepage-oriented (0.30/0.70) scenarios tested here.
- The GWO-RF surrogate predicts FOS more reliably than Q. The weakest model is Q for the 35 m, 1V:1.5H configuration, with testing $R^2 = 0.46$. The surrogate-based dense check should consequently be regarded as a consistency assessment rather than an independent verification of the finite-element Pareto front, and the finite-element Pareto sets themselves remain the primary design result.
- Future work should extend d/N and h/H beyond the current bounds, use cross-validated or out-of-bag surrogate tuning, verify representative Pareto/TOPSIS designs with new ABAQUS runs, and include transient and unsaturated seepage effects.

References

Al-Janabi AMS, Dibs H, Sammen SS, Yusuf B, Ikram RMA, Alzuhairy SH, Kisi O (2025) Comparison analysis of seepage through homogenous embankment dams using physical, mathematical and numerical models. *Arabian Journal for Science and Engineering* 50:8143–8152. https://doi.org/10.1007/s13369-024-09224-x

Al-Juboori M, Datta B (2019) Optimum design of hydraulic water retaining structures incorporating uncertainty in estimating heterogeneous hydraulic conductivity utilizing stochastic ensemble surrogate models within a multi-objective multi-realisation optimisation model. *Journal of Computational Design and Engineering* 6(3):296–315. https://doi.org/10.1016/j.jcde.2018.12.003

Amieur R, Djehiche A, Boumaaza CL, Gafsi M, Lalmi D (2023) Effect location of vertical drain on seepage and stability in homogenous earth dams. *International Journal of Sustainable Development and Planning* 18:2643–2653. https://doi.org/10.18280/ijsdp.180903

Arabet L, Belaabed F, Benbouza A, Malaoui R (2025) Hybrid machine learning and bio-inspired optimization for accurate safety factor prediction in Earth dams. *Journal of Umm Al-Qura University for Engineering and Architecture*. https://doi.org/10.1007/s43995-025-00271-5

Bardhan A, Suman SK, Kumar S, Chaudhary L, Asteris PG (2024) An efficient framework of optimized ensemble paradigm for estimating resilient modulus of subgrades. *Transportation Geotechnics* 48:101315. https://doi.org/10.1016/j.trgeo.2024.101315

Breiman L (2001) Random forests. *Machine Learning* 45:5–32. https://doi.org/10.1023/A:1010933404324

Calamak M, Yilmaz AN, Yanmaz AM (2018) Performance evaluation of internal drains of earth dams. *Journal of Performance of Constructed Facilities* 32:04018085. https://doi.org/10.1061/(ASCE)CF.1943-5509.0001232

Chahar BR (2004) Determination of length of a horizontal drain in homogeneous earth dams. *Journal of Irrigation and Drainage Engineering* 130(6):530–536. https://doi.org/10.1061/(ASCE)0733-9437(2004)130:6(530)

Charrak H, Taleb HA, Louallia H, Bouguerba SE (2025) Comparative analysis of horizontal and pipe drains in earth dams: Optimizing seepage control and stability (case study). *Environmental Earth Sciences* 84:39. https://doi.org/10.1007/s12665-024-12065-4

Chen X, Xu Y, Guo H, Hu S, Gu C, Hu J, Qin X, Guo J (2024) Comprehensive evaluation of dam seepage safety combining deep learning with Dempster-Shafer evidence theory. *Measurement* 226:114172. https://doi.org/10.1016/j.measurement.2024.114172

Dawson EM, Roth WH, Drescher A (1999) Slope stability analysis by strength reduction. *Géotechnique* 49(6):835–840. https://doi.org/10.1680/geot.1999.49.6.835

Deb K, Pratap A, Agarwal S, Meyarivan T (2002) A fast and elitist multiobjective genetic algorithm: NSGA-II. *IEEE Transactions on Evolutionary Computation* 6(2):182–197. https://doi.org/10.1109/4235.996017

EL-Molla DA, Kilit M (2026) Seepage control, detection, and treatment in embankment dams: A state-of-the-art review. *Arabian Journal for Science and Engineering* 51:3823–3849. https://doi.org/10.1007/s13369-025-10185-y

Fawzy MA, Hassan NAA, Saad NY et al (2024) Evaluating the effect of different diaphragm wall cracking scenarios on seepage and slope stability in Earth dams using experimental and numerical modeling approaches. *Beni-Suef University Journal of Basic and Applied Sciences* 13:66. https://doi.org/10.1186/s43088-024-00523-8

Fontanella E, Pagano L, Desideri A (2025) Pore water pressure measurements as indicator or precursor of core hydraulic alteration in zoned Earth dams. *Bulletin of Engineering Geology and the Environment* 84:554. https://doi.org/10.1007/s10064-025-04538-y

Haghdoost M, Lakzian E, Norouzi R, Abraham J, Sajjadi SM, Ahadiyan J (2023) Numerical simulation using the finite element method to investigate the effect of internal cutoff walls on seepage and hydraulic gradients in homogeneous earth dams. *Modeling Earth Systems and Environment* 9:3851–3864. https://doi.org/10.1007/s40808-023-01755-w

Hassan WH, Atshan TT, Thiab RF (2024) Effect of drain pipes on seepage and slope stability through a zoned earth dam. *Open Engineering* 14(1):20240040. https://doi.org/10.1515/eng-2024-0040

Hassan WH, Hussein HH, Khashan DH, Alshammari MH, Nile BK (2022) Application of the coupled simulation-optimization method for the optimum cut-off design under a hydraulic structure. *Water Resources Management* 36:4619–4636. https://doi.org/10.1007/s11269-022-03269-z

Hassan WH, Hussein HH, Khashan DH, Nile BK (2023) Optimum hydraulic design of cutoff under hydraulic structures using the simulation-optimization method. *Modeling Earth Systems and Environment* 9:493–505. https://doi.org/10.1007/s40808-022-01511-6

He P, Wu W (2023) Levy flight-improved grey wolf optimizer algorithm-based support vector regression model for dam deformation prediction. *Frontiers in Earth Science* 11:1122937. https://doi.org/10.3389/feart.2023.1122937

Hodson TO (2022) Root-mean-square error (RMSE) or mean absolute error (MAE): When to use them or not. *Geoscientific Model Development* 15:5481–5487. https://doi.org/10.5194/gmd-15-5481-2022

Huang F, Xiong H, Chen S, Lv Z, Huang J, Chang Z, Catani F (2023) Slope stability prediction based on a long short-term memory neural network: Comparisons with convolutional neural networks, support vector machines and random forest models. *International Journal of Coal Science & Technology* 10:18. https://doi.org/10.1007/s40789-023-00579-4

Huang H, Zhu J, Wu Z, Chen J, Tian J (2025) System reliability analysis of slope stability of earth rock dams based on finite element strength reduction method. *Applied Sciences* 15(9):4672. https://doi.org/10.3390/app15094672

Hwang CL, Yoon K (1981) *Multiple Attribute Decision Making: Methods and Applications*. Springer-Verlag. https://doi.org/10.1007/978-3-642-48318-9

Kadkhodaei MH, Ghasemi E, Fazel MH (2025) Slope stability prediction of circular mode failure by machine learning models based on Bayesian optimizer. *Journal of Mountain Science* 22(4):1482–1498. https://doi.org/10.1007/s11629-024-8864-9

Lee HJ, Kim I, Chung CK (2024) Assessing the progress of internal instability of fill dam material in South Korea through long-term seepage tests. *Bulletin of Engineering Geology and the Environment* 83:182. https://doi.org/10.1007/s10064-024-03662-5

Liu G, Zhou Z, Zhang J, Jiang G, Mi W (2024) Seepage and stability analysis of earth dams downstream slopes, considering hysteresis in soil-water characteristic curves under reservoir water level fluctuations. *Water* 16(13):1811. https://doi.org/10.3390/w16131811

Mirjalili S, Mirjalili SM, Lewis A (2014) Grey wolf optimizer. *Advances in Engineering Software* 69:46–61. https://doi.org/10.1016/j.advengsoft.2013.12.007

Mostafa MM, Zhenzhong S (2023a) Numerical study concerning the different drainage systems in earth dams. *Journal of Hydraulic Structures* 9:101–117. https://doi.org/10.22055/jhs.2023.44272.1258

Mostafa MM, Zhenzhong S (2023b) Effect of zones' dimensions and geometry on seepage through zoned earth dams. *Journal of Engineering and Applied Science* 70:46. https://doi.org/10.1186/s44147-023-00223-7

Mouyeaux A, Carvajal C, Nicot F, Wautier A, Peyras L (2023) Stability analysis of earth dam slopes based on the second-order work criterion in finite element modeling. *Geotechnics* 3(4):1117–1134. https://doi.org/10.3390/geotechnics3040061

Parsaie A, Avazpour F, Afaridegan E (2025) Numerical modeling of optimal location of drainage and cutoff wall under small concrete dams. *Applied Water Science* 15:76. https://doi.org/10.1007/s13201-025-02422-4

Pourbeirak S, Johari A, Aghaee Daneshvar F, Habibagahi G (2026) Reliability analysis of seepage in earth dam considering saturated-unsaturated flow: A case study. *Computers and Geotechnics* 191:107797. https://doi.org/10.1016/j.compgeo.2025.107797

Radzicki K, Stoliński M (2024) Seepage monitoring and leaks detection along an earth dam with a multi-sensor thermal-active system. *Bulletin of Engineering Geology and the Environment* 83:362. https://doi.org/10.1007/s10064-024-03826-3

Refaiy AR, AboulAtta NM, Saad NY, El-Molla DA (2021) Modeling the effect of downstream drain geometry on seepage through earth dams. *Ain Shams Engineering Journal* 12(3):2511–2531. https://doi.org/10.1016/j.asej.2021.02.011

Rehamnia I, Mahdavi-Meymand A (2025) Advancing reservoir water level predictions: Evaluating conventional, ensemble and integrated swarm machine learning approaches. *Water Resources Management* 39:779–794. https://doi.org/10.1007/s11269-024-03990-x

Siacara AT, Napa-García GF, Beck AT et al (2022) Reliability analysis of an earth dam in operating conditions using direct coupling. *SN Applied Sciences* 4:99. https://doi.org/10.1007/s42452-022-04980-7

Soualhi M, Benmebarek N (2022) Experimental and numerical analyzes of parallel drains series performance in earth dams. *Modeling Earth Systems and Environment* 8:4815–4828. https://doi.org/10.1007/s40808-022-01482-8

Wang M, Zhao G, Wang S (2024) Hybrid random forest models optimized by Sparrow search algorithm (SSA) and Harris hawk optimization algorithm (HHO) for slope stability prediction. *Transportation Geotechnics* 48:101305. https://doi.org/10.1016/j.trgeo.2024.101305

Wise J, Hunt S, Al Dushaishi M (2023) Prediction of earth dam seepage using a transient thermal finite element model. *Water* 15(7):1423. https://doi.org/10.3390/w15071423

Yu F, Zhang X, Wu SC, Feng Y, Zhang L (2025) Slope stability evaluation and prediction based on KTAN coupling model and Monte Carlo method. *Journal of Computational Science* 88:102580. https://doi.org/10.1016/j.jocs.2025.102580

Zakaria SMS, Mahmood MT (2023) Comparison seepage performance for different drainage systems of rainwater harvesting dam. *International Journal of Safety and Security Engineering* 13:301–316. https://doi.org/10.18280/ijsse.130212

Statements and Declarations

Funding. The authors declare that no funds, grants, or other support were received during the preparation of this manuscript.

Competing interests The authors have no relevant financial or non-financial interests to disclose.

Author contributions. All authors contributed to the study conception and design. Material preparation, data collection and analysis were performed by [A.R.M]. The first draft of the manuscript was written by [B.B] and all authors commented on previous versions of the manuscript. All authors read and approved the final manuscript.

Data availability. The finite-element results database (design variables, FOS and Q for all simulated configurations) analysed during the current study is available from the corresponding author on reasonable request.